Long-term measurements of atmospheric point spread functions over littoral waters, as determined by atmospheric turbulence

Arie N. de Jong[a], Piet B.W. Schwering[a], Koen W. Benoist[a]
Willem H. Gunter[b], George Vrahimis[b], Faith J. October[b]
[a]TNO, PO Box 96864, The Hague, The Netherlands
[b]Institute for Maritime Technology (IMT), Simon's Town 7995, South Africa

ABSTRACT

During the FATMOSE trial, held over the False Bay (South Africa) from November 2009 until October 2010, day and night (24/7) high resolution images were collected of point sources at a range of 15.7 km. Simultaneously, data were collected on atmospheric parameters, as relevant for the turbulence conditions: air- and sea temperature, windspeed, relative humidity and the structure parameter for refractive index: C_n^2. The data provide statistical information on the mean value and the variance of the atmospheric point spread function and the associated modulation transfer function during series of consecutive frames. This information allows the prediction of the range performance for a given sensor, target and atmospheric condition, which is of great importance for the user of optical sensors in related operational areas and for the developers of image processing algorithms. In addition the occurrence of "lucky shots" in series of frames is investigated: occasional frames with locally small blur spots. The simultaneously measured short exposure blur and the beam wander are compared with simultaneously collected scintillation data along the same path and the C_n^2 data from a locally installed scintillometer. By using two vertically separated sources, the correlation is determined between the beam wander in their images, providing information on the spatial extension of the atmospheric turbulence (eddy size). Examples are shown of the appearance of the blur spot, including skewness and astigmatism effects, which manifest themselves in the third moment of the spot and its distortion. An example is given of an experiment for determining the range performance for a given camera and a bar target on an outgoing boat in the False Bay.

KEYWORDS: littoral waters, atmospheric MTF, turbulence, scintillation, range performance

1. INTRODUCTION

An important application of electro-optical systems is surveillance in coastal areas by using shore-based or ship-borne sensors. Targets of interest are generally small (boats) with people on board. Requirements for the sensors include the ability of counting numbers of people and determination of the presence of (types of) weapons at ranges, as long as possible. If in this kind of application a resolution is taken of 10 cm on a target at a range of 10 km, an angular resolution of 10 μradian is required. This type of resolution can easily be achieved with modern diffraction limited camera systems, operating in the visual band, having apertures of about 7 cm. A big question is however, if the atmosphere allows this kind of range due to its extinction coefficient (km^{-1}) and to its blur, which increases with range. In a previous trial in the False Bay in 2007, it was found that at ranges of 10 km and more, the atmospheric blur can easily be the dominant factor, limiting the spatial resolution [1], [2]. This is also predicted by the theory, based upon the atmospheric coherence length r_0, introduced by Fried [3] and further applied in the atmospheric modulation transfer function (MTF) by Holst [4]. The knowledge of C_n^2 along the path is required in applying these formulae. An alternative is to predict C_n^2, as output of a marine boundary layer model (EOSTAR), based upon bulk input parameters [5].

One has to realise that these predictions have a limited validity in coastal and bay areas due to potential inhomogeneous atmospheric conditions along the path. In the False Bay the water temperature may vary more than two degrees due to tidal currents, leading to variations in ASTD (Air Sea Temperature Difference) and constitutions of the boundary layer. After the first experiment in 2007 at IMT [1], the possibility came up to arrange the FATMOSE trial in the same area, but with improved equipment for collecting a more extensive set of atmospheric and point target data. These data include those from local weather stations, a midpath visibility meter, an infrared radiometer for the measurement of the surface temperature of the water and a scintillometer (for collecting C_n^2 data), as described previously [6]. Simultaneously data

Infrared Imaging Systems: Design, Analysis, Modeling, and Testing XXIII, edited by Gerald C. Holst, Keith A. Krapels,
Proc. of SPIE Vol. 8355, 83550M · © 2012 SPIE · CCC code: 0277-786X/12/$18 · doi: 10.1117/12.917718

were collected on atmospheric transmission, refraction and blur for a range of 15.7 km. The multiband transmission data were used to retrieve particle size distributions and to compare the in-situ visibility data with the transmission data in the same spectral band [7]. The refraction data were used to validate the vertical temperature profiles and the associated heat, momentum and moisture transfer (by turbulence) in the marine boundary layer, as predicted from the Monin-Obukhov theory and applied in the EOSTAR model [8].

In this paper blur data are presented and discussed, collected with a high resolution camera system. Details of this system are presented as well as the method of analysis. The blur data consist of simultaneously collected short exposure values and beam wander for two vertically separated sources. In addition the large dynamic range of the camera system (10 bits) allowed retrieval of the scintillation index. Due to the long duration of the campaign, a good feeling could be obtained of the blur statistics over the period of nearly a year. Correlation of the blur data with weather data in general and with C_n^2 in particular, has been investigated and is presented. In the section on beam wander, the correlation between the image motion of the two sources is presented. This information is useful for signal processing applications. In the next section an example is given of a direct and illustrative way for determining the resolution of an EO sensor system, as executed in the False Bay from the roof of the IMT building.

2. DIRECT RESOLUTION EXPERIMENT

A direct and simple way to check the influence of atmospheric turbulence on sensor resolution is the use of a bar target, moving out on a small boat to significant ranges. During FATMOSE, such an experiment was carried out, where a 5 bar target was mounted on the Sealab, sailing out from about 300 m to about 5000 m. The bars had a width of 10 cm each, corresponding to 5 cycles per meter. An Arecont camera with 300 mm lens was used, collecting 16 frames per second. This camera, working in the visual band, has a detector centre to centre distance of 10.7 µrad. This implies that the MTF of the camera (ignoring the optical MTF) is dropping down to zero, following a sinc function, at a spatial frequency of 93.5 c/mrad. The Nyquist frequency (where aliasing starts) is half of that: 46.8 c/mrad. An estimation of the optical MTF was made from short range imagery, such as shown in Figure 1 (left image), where the total camera MTF was obtained via the edge response of the bars. Next the range was determined (4100 m), at which the resolution of the bars became impossible or poor, as illustrated in the other pictures of Figure 1.

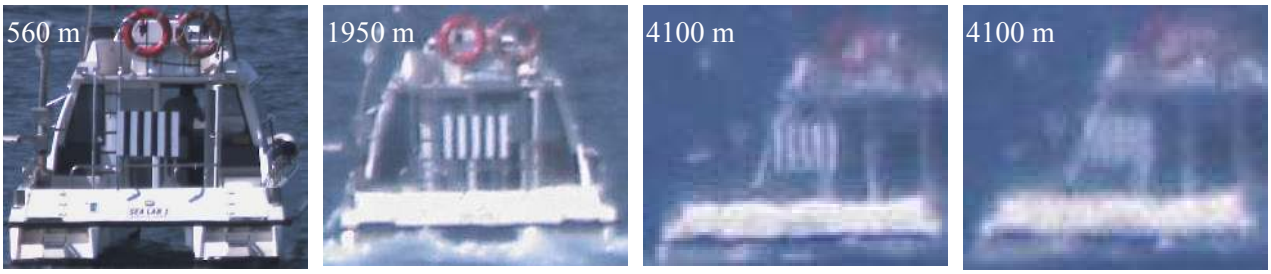

Figure 1. Imagery of an outbound small boat in the False Bay with 5-bar target at various ranges on 5 Oct. 2010-15.00.

From the estimated total camera MTF follows a value of 0.05 for a spatial frequency of 44 c/mrad, which is just below the Nyquist frequency. It is noted that in this MTF, lens aberrations and diffraction are standard contributions, but that a potential (unknown) contribution to de-focussing may be present. The corresponding spatial frequency of the bars at 4100 m is 20.5 c/mrad (also assuming a contrast of 0.05), which is about a factor two below the capability of the camera. For the interpretation of "seeing" the bars, it is noted that they are just discernable in a limited number of consecutive frames, occurring randomly, as shown in the two pictures on the right in Figure 1. Apparently the blur spot is varying in size from frame to frame and seeing the bars is just a matter of luck. It is of interest that when the bars are discernable, one can see them as a whole pattern, indicating that the isoplanatic area is in this case bigger than the bar target. It has to be mentioned however that the contrast reduction of the bars with range is partly caused by atmospheric transmission loss. During the experiment the visibility, measured at the Roman Rock lighthouse (1.8 km from IMT) was 8 km, which implies a transmission level of 0.14 for a range of 4.1 km. So the bar contrast for the bars only is 0.357. If the visibility would have been 16 km, one would have found a recognition range of 5260 m at a spatial frequency of 26.3 c/mrad.

This makes clear that this kind of experiment is only indicative and depending on the local weather conditions. Actually the visibility was quite drastically changing during the afternoon of the experiment, while a big fog cloud was present beyond a range of 7 km, which follows from the simultaneously measured transmission over the whole range of 15.7 km. Another interesting issue is a comparison of the measured blur with predictions from the Fried theory. The atmospheric $MTF_t(f)$ as function of the spatial frequency f due to turbulence (plane wave) is given by:

$$MTF_t(f)=\exp\{-(f/f_c)^{5/3}\} \quad \text{with} \quad f_c=r_0/(2.1\lambda) \quad \text{and} \quad r_0=2.1\{1.46(2\pi/\lambda)^2C_n^2R\}^{-3/5} \qquad (1)$$

where λ is the wavelength and R the range. The cut-off spatial frequency f_c is the point in the MTF, where its value is decreased to 1/e and is directly related to the definition of blur. For $\lambda=0.55*10^{-6}$ m, $R=4.1*10^3$ m and a measured value of $C_n^2=6.3*10^{-15}$ $m^{-2/3}$ (measured at Roman Rock), r_0 is found to be: $12.8*10^{-3}$ m and f_c: 11.1 c/mrad. From (1) follows that the point where the MTF becomes 0.05 corresponds to a spatial frequency of 21.4 c/mrad, which corresponds quite good with the result of the measurement, presented before.

3. EQUIPMENT AND SET-UP

It is clear that the use of a bar pattern for the determination of sensor resolution, as described in the previous section, is illustrative but less suitable for long term studies. The subjective nature and the influence of atmospheric transmission are other drawbacks of the method, which is only working in daylight. For FATMOSE it was decided therefore to use small searchlamps with the advantage of their high contrast with the background. In the lamps (the same as during the POLLEX trial [9] for a range of 34 km), 12 V (50 Watt) halogen tubes are positioned in the focus of a parabolic reflector with a diameter of 150 mm and a focal length of 30 mm. The radiant intensity I_s for the full aperture in the spectral band 0.7-1.0 μm is about 2 kW/sr.

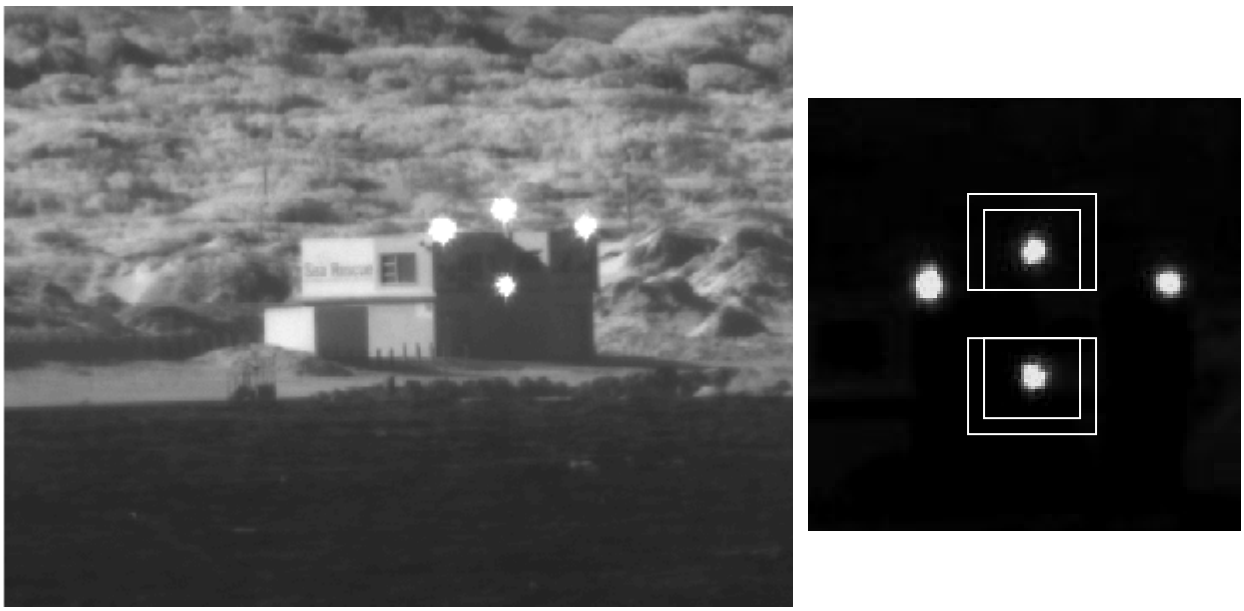

Figure 2. Image of the four sources and their background on the roof of the NSRI building in Strandfontein at 15.7 km from IMT, Simonstown. On the right the two major sources with the analysis windows around the spots.

In this way a sufficient contrast was created with the background, noting the ratio of the detector exposure by the source and the background radiance W_b (W/m^2sr), approximately given by: $(\tau_a\tau_s\eta I_s)/(R^2\delta^2W_b)$, where R is the range, τ_a and τ_s are the atmospheric respectively source window transmission and δ is the detector angular subtense. The efficiency η is the fraction of the point source radiation, falling on one detector element. It has to be taken into account that the source window transmission degrades with time, due to exposure with sea salt. By taking: $R=15.7x10^3$ m, $\delta=5x10^{-6}$ radian,

η=0.25 and W_b=10 W/m^{2}sr (daytime), the ratio becomes about 800 in the case that the product $\tau_a\tau_s$ is 0.1, favorable for having a good daytime contrast. Figure 2 (left) shows the four sources on top of the Sea Rescue building in Strandfontein with a longer integration time (10 ms) of the Marlin camera. The two central sources were located at a height of 9.7 and 5.8 m above mean sea level. The (modulated) left source (used for transmissometry) and the right source (for refraction studies) were mounted at an altitude of 8.7 m. In front of the central sources, limiting apertures of 90 mm were applied to avoid saturation of the camera.

The receiving telescope was an 8-inch, f/10 Celestron with a focal length of 2.03 m. In its focal plane a 10 bits Marlin F-033B camera was mounted, supplied with a near IR filter (0.7-1.0 µm). The detector size of 9.9x9.9 µm corresponds to a detector angular subtense δ of about 5x5 µrad. The Marlin camera provides images with 640x480 pixels at a frame rate of 30 Hz and a dynamic range of 10 bits. The integration time can be set from 100 to 33000 µs. Telescope and camera were mounted behind an open window in the IMT building at an altitude of 14.5 m above mean sea level. The total field of view of the camera was 3.2x2.4 mrad, which is somewhat small. In case of severe refraction conditions the spot may run out of this field of view. Every 5 minutes a series of 150 frames, containing 90 Mb of data, was collected and stored on a PC. For the Modulation Transfer Functions (MTFs) of the Telescope (F_0), the detector (F_c) and the source (F_s) the following relations are used:

$$F_0=(2/\pi)*[\arccos(f/f_0)-(f/f_0)*\{1-(f/f_0)^2\}^{0.5}] \qquad F_c=\{\sin(\pi f/f_c)\}/(\pi f/f_c) \qquad F_s=2*J_1(f/f_s)/(f/f_s) \qquad (2)$$

where $f_0=D_t/\lambda$ =250 c/mr, $f_c=FL_t/d_c$=200 c/mr and $f_s=R/(\pi D_s)$=55.5 c/mr. Here D_t and FL_t are the diameter and focal length of the telescope, d_c the detector size and D_s the diameter of the source. F_0 and the product $F_0*F_c*F_s$ are shown in Figure 3 together with a Gaussian curve $F(f)=\exp\{-(f/78)^2\}$, that fits nicely to the product. This means that in the spatial domain a corresponding Gaussian line spread function (LSF) can be specified for the total system: $L(x)=\exp\{-(x/\sigma_s)^2/2\}$ with $\sigma_s=1/(\pi*78\sqrt{2})$ mrad=2.89 µrad, to be interpreted as a measure for the blur of the measurement set-up.

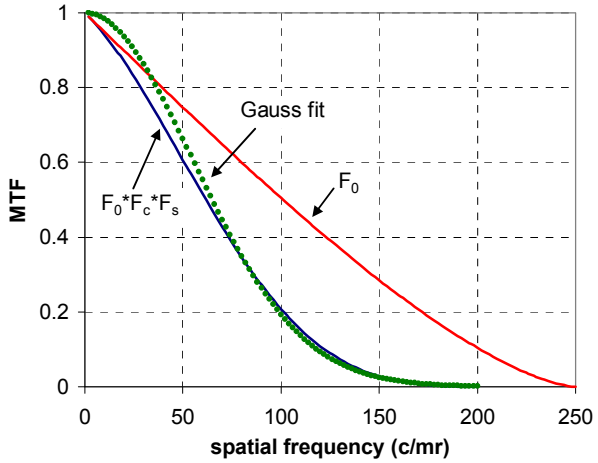

Figure 3. Modulation Transfer Functions (MTF) of the optical components of the FATMOSE blur measurement set-up: F_0 (telescope), F_c (detector) and F_s (source, 9 cm diameter)

It is noted, that the blur of the telescope, as given in equation (2) is considered as being caused by diffraction of the aperture only. Measurements at TNO confirmed that the telescope is nearly diffraction limited. In practical applications however, residual blur may be caused by non-proper focussing. Especially in situations, where the image is blurred by atmospheric turbulence, proper focus is hard to verify. In the set-up at IMT, focussing was done during moments of low turbulence, while looking back at lucky shots in series of images.

The direction of observation during FATMOSE was North-East, which is about perpendicular to the two prevailing wind directions: South-East and North-West. This fact is favourable for the interpretation of turbulence effects, considering the "frozen turbulence", being blown directly through the line of sight. Turbulence theories are generally valid for static atmospheric conditions (spatial effects), while the measurements deliver temporal data [10]. The windspeed at the False

Bay site is generally moderate to strong, as can be observed from the histogram in Figure 4. Together with the ASTD, for which also a histogram is shown in Figure 4, the windspeed is responsible for the strength of atmospheric turbulence [8]. Both were measured at the Roman Rock lighthouse, about 1.8 km from IMT, close to the line of sight. It is noted, that windspeeds up to 20 m/s do occur, while the maximum probability of occurrence for ASTD is close to zero, indicating that the atmosphere is most of the time of maritime nature. The ASTD was measured, using a standard device for the air temperature and an IR radiometer for the sea temperature.

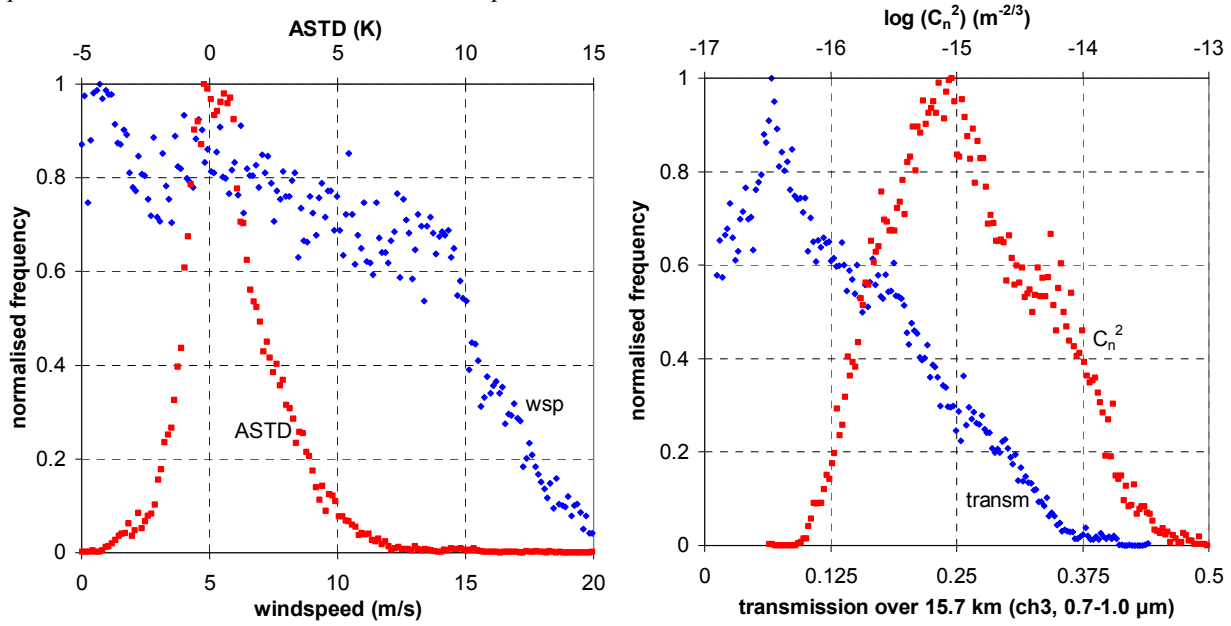

Figure 4. Histograms of ASTD, windspeed, log (C_n^2) and transmission for about 250 days of collected data, spread over the FATMOSE period

Other histograms in Figure 4 concern C_n^2, measured with a standard BLS-900 scintillometer between IMT and Roman Rock, and the transmission in one of the Celestron transmission bands along the 15.7 km path, measured with the MSRT transmissometer [7]. These data show that the maximum probability of occurrence for C_n^2 in the False Bay is 10^{-15} $m^{-2/3}$. This value is significantly lower than for overland trajectories or for the littoral area (Baltic Sea), as published by Weiss-Wrana [11], which means that in the False Bay the atmospheric blur should be statistically smaller than in the Baltic Sea.

4. METHOD OF ANALYSIS

For each image from the Celestron camera system two windows were set around the central spots, as shown in Figure 2 (right). The size of the windows was generally much bigger than the spot size and roughly between 30 and 50 pixels in both X and Y direction. Next, background areas were defined with a width of 10 pixels, covering three sides the window of each spot. The background areas did not cover the side, aiming towards the other spot to avoid eventual light of one spot entering the background window of the other spot. The mean bit level and its standard deviation of the background areas were calculated. In order to eliminate background noise effects on the spot size, a threshold was set of 3 times the standard deviation above the mean background level. The next step concerns the calculation of the centroid of the spot (as rising above the threshold) and its second and third moment according to the relations:

$$x_c=\iint xI(x,y)dxdy/\iint I(x,y)dxdy \quad M_{20}=\iint (x-x_c)^2 I(x,y)dxdy/\iint I(x,y)dxdy \quad M_{30}=\iint (x-x_c)^3 I(x,y)dxdy/\iint I(x,y)dxdy \qquad (3)$$

for the X direction and similar relations for the Y direction. Here I(x,y) is the bit level distribution over the spot area and x_c the "centre of gravity" of the spot in X direction. M_{20} and M_{30} are the variance, respectively the skewness of the blur spot in X direction. Similarly y_c, M_{02} and M_{03} are defined for the Y direction. Initially x and y are used as pixel numbers of the Marlin chip, that have to be converted into µrad in the object space by multiplying with a factor 5.

The measured blur σ_t is defined as the geometrical average of the horizontal and vertical blur: $\sigma_t=\sqrt{(\sqrt{M_{20}}*\sqrt{M_{02}})}$. In order to obtain the atmospheric blur σ_a, the system blur σ_s has to be subtracted quadratically: $\sigma_a=\sqrt{(\sigma_t^2-\sigma_s^2)}$. The LSFs L(x) and L(y) in X and Y direction, the integrated intensity I_i and the mean beam wander (BW) follow from the relations:

$$L(x)=\int I(x,y)dy \qquad L(y)=\int I(x,y)dx \qquad I_i=\iint I(x,y)dxdy \qquad BW=<\sqrt{\{(x_n-x_c)2+(y_n-y_c)2\}}> \ (n=1...150) \qquad (4)$$

where x_n and y_n are the gravity centres for the n^{th} frame and the mean of the BW is taken for each series of 150 frames. Examples of blurred spots and their associated LSFs are shown in Figure 5, with a small blur on 17/12-10.00 (left) and a large blur on 28/3-13.00 (right). The LSFs are fairly close to Gaussian functions, which means that the corresponding MTFs are also close to Gaussian functions, which is in agreement with the theory (Fried, formula (1))

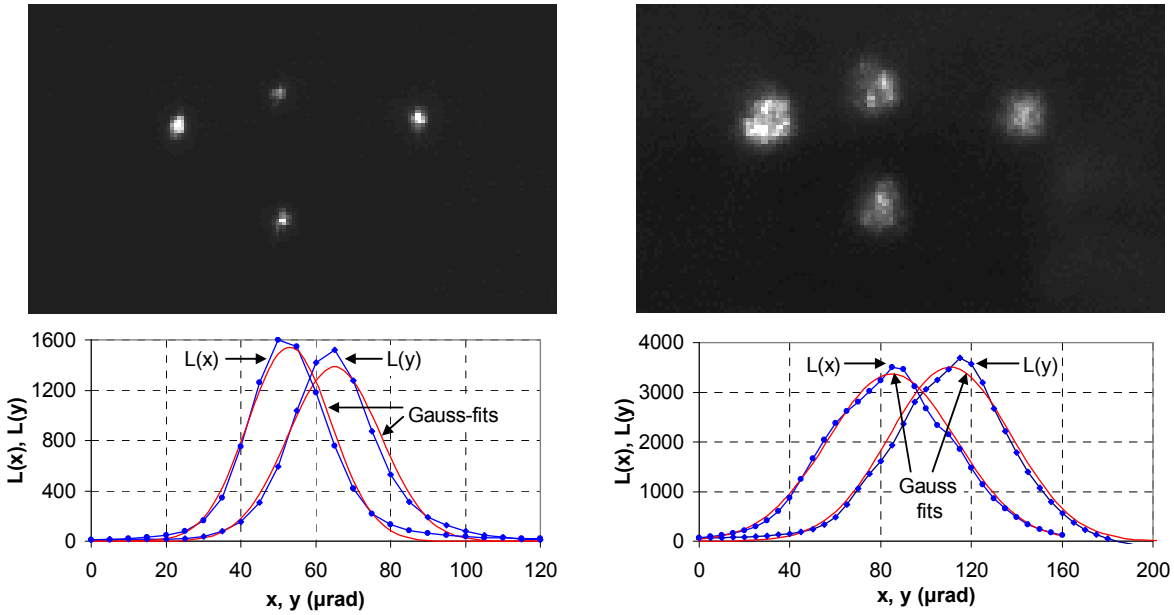

Figure 5. Examples of small and large atmospheric blur and their associated LSFs (including Gauss-fits)

It is noted that the Matlab script for calculating the relations (3) and (4), including the mean and standard deviations of σ_t, I_i and BW for the series of 150 frames, did run in real time in the 5 minutes between two successive data collection points. An algorithm was applied to keep each centre of gravity in the middle of the window to avoid the running out of the window in case of changing refraction conditions. When the upper window was touching the topside of the Marlin field of view, the programme stopped. In this case the upper window was moved to the lower source. Sometimes both windows were taken around the same source (but with different background areas). This procedure allowed a check of the influence of these different background areas. All calculations were repeated afterwards, where sometimes the bigger sources (Topcon, 15 cm diameter or MSRT, 20 cm diameter) were used, in which case different values for the system blur σ_s have to be used (3.63 µrad respectively 4.50 µrad).

A number of problems or errors may occur during the data collection and LSF calculation procedure. The visibility has to be sufficient for the creation of a suitable contrast. As published in a previous study [7], the probability of atmospheric transmissions above 5% is 80% in the False Bay. This kind of transmission value is considered to be the limit, below which the contrast is too small. In cases of small contrast, only the top part of the point spread function rises above the threshold, resulting in a too small blur value. Signals were sometimes saturated (maximum bit level is 1024) when the atmospheric transmission (combined with a long integration time) was high. Similarly the integration time had to be turned down after cleaning the source window, to avoid saturation. In these cases the measured blur value was too high. Another problem is the background radiance in bright sunshine conditions, combined with low atmospheric transmission or for some frames with a small intensity (due to turbulence). Again the blur value is too small in these cases. One way to check the validity of the blur value is to look at the ratio of its standard deviation and its mean value (should be <1/3).

For the interpretation of the blur value, one has to realise that the optical resolution could be considered in terms of the atmospheric MTF, as shown in section 2. The measured LSF: $L(a,x)=\exp\{-(x/\sigma_a)^2/2\}$ is corresponding to an atmospheric MTF of $F(f)=\exp\{-2(\pi\sigma_a f)^2\}$, characterised by the value of σ_a at the 1/e point: $f=1/(\pi\sigma_a\sqrt{2})$. Another way to interpret the value of σ_a is to look at the angular separation between two identical Gaussian functions with variance σ_a^2, that are just discernable by an observer. Following this method, earlier applied to laboratory measurements of infrared cameras [12], it is found that an angular separation of $2.43\sigma_a$, leads to a signal dip of 10% in between of the two peaks. This contrast is considered to be enough for discrimination of the peaks, similar to the classical way of defining the optical resolution of a diffraction limited optical system (where the signal dip is about 20% for a separation distance, equal to the diameter of the first diffraction ring).

5. GENERAL DATA REVIEW

Useful Celestron data could be collected for 250 out of the 315 FATMOSE days (80%). Some days were lost because of technical reasons and on other days no meaningful data could be collected due to poor meteorological conditions such as poor visibility, or extreme refraction or turbulence conditions. The vast amount of data allows the selection of events in the campaign, where the weather conditions did not change too much for at least a few hours. One has to be careful that the selected data contain a representative set of weather conditions with similar statistical behaviour as those presented in Figure 4 for the whole period. In this manner a selection was made of 475 events, spread over day and night and over all seasons, for which the measured blur, calculated according to the procedure, described in the previous section, is shown in Figure 6. In addition this figure shows the simultaneously measured C_n^2 data, of which the values are spread around 10^{-15} $m^{-2/3}$ as in Figure 4 (right). The blur data (corrected for sensor and system blur) are spread around 20 µrad, which value corresponds to an optical resolution of 2.43*20=49 µrad (for an atmospheric path of 15.7 km). The corresponding 1/e point of the atmospheric MTF is located at a spatial frequency of $f=1/(\pi\sigma_a\sqrt{2})=11.3$ c/mrad. It also means that the atmospheric MTF is reduced to 5% at a spatial frequency of 19.5 c/mrad. In other words: atmospheric turbulence makes the discrimination of spatial details smaller than 0.8 m at ranges of 15.7 km and more impossible in many cases.

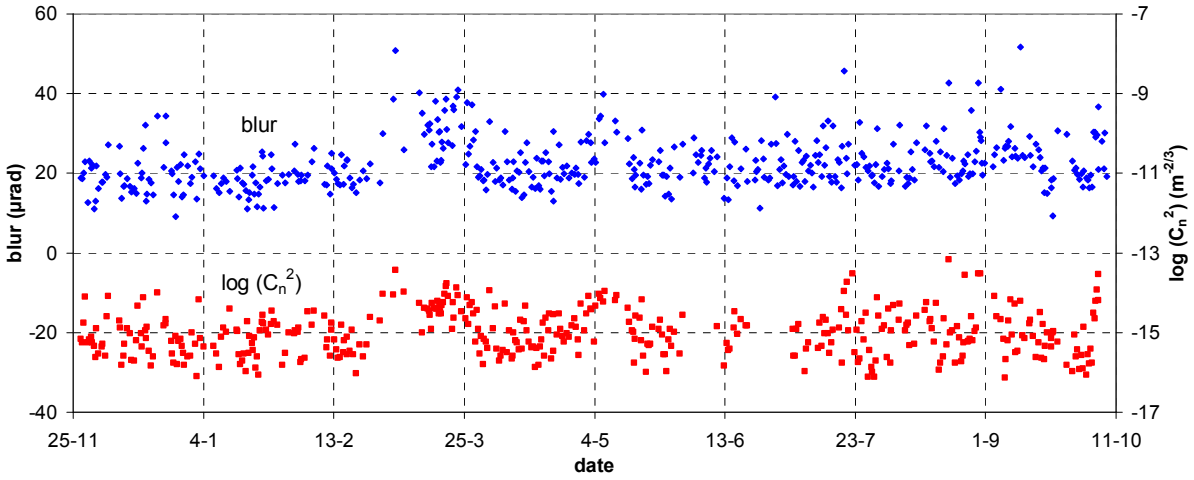

Figure 6. Series of selected blur measurements (including C_n^2 data) during the FATMOSE measurement period

During the preparation of the presented blur data each image series had to be carefully treated by eliminating suspicious frames, as discussed previously (e.g. too big ratio of standard deviation and mean blur). In some occasions extreme blur values were found, such as 82 µrad on the 22nd of July at 05.30. These data are not included as they did last only for a few minutes. On the other hand, each series of 150 frames contained frames with smaller blurs, as will be discussed in the next section. It is noted that for 17 data points in Figure 6, the blur values were obtained from the Topcon camera, because the spot was outside the field of view of the Celestron camera. The blur data, shown in Figure 6, concern short exposure data, as the integration time of the Marlin camera was less than 1 ms in all cases. The beam wander BW, of which the magnitude varies similar with time as the blur, was calculated for the same selection. Histograms for the blur and BW data of the selected events are shown in Figure 7.

This figure shows that 50% of the blur values is bigger than 20 µrad, while 50% of the BW data is bigger than 8 µrad. Blur values as small as 10 µrad were occasionally measured, for example on 26/12 11.00. The blur values for the spots, shown in Figure 5 were found to be 12.9 respectively 30.5 µrad. In some cases (less than 1% of the time) blur values of more than 45 µrad were measured, combined with a BW of more than 25 µrad. It was found that the statistics of the second spot were mostly similar to those of the first spot. Only in cases that background radiance hampered one of the chosen windows, deviations in blur size of about 20% were found.

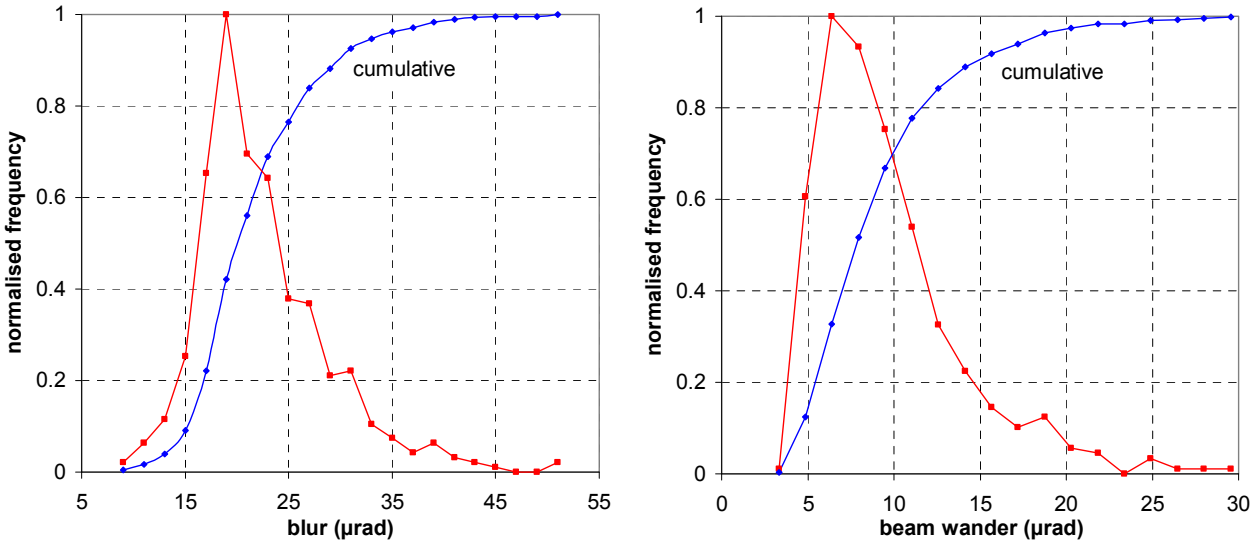

Figure 7. Histograms of blur and beam wander values for the selected data series

Of course the analysis was not limited to the selected data. Individual series of 150 frames were investigated, as well as series, covering a few days with significant and slowly varying weather conditions. In the following sections, examples of them will be presented and discussed. This will include an analysis of the correlation between the different turbulence and weather parameters.

6. SINGLE SERIES OF 150 FRAMES

In this section some of the main characteristics of a typical "150 frame"series are described. Figure 8 shows the temporal behaviour (5 seconds) of the blur and beam wander of the lowest central source with mean values of 4.26 respectively 1.69 pixels and standard deviations of 0.33 respectively 0.88 pixels (1 pixel = 5 µrad). It is observed that blur and beam

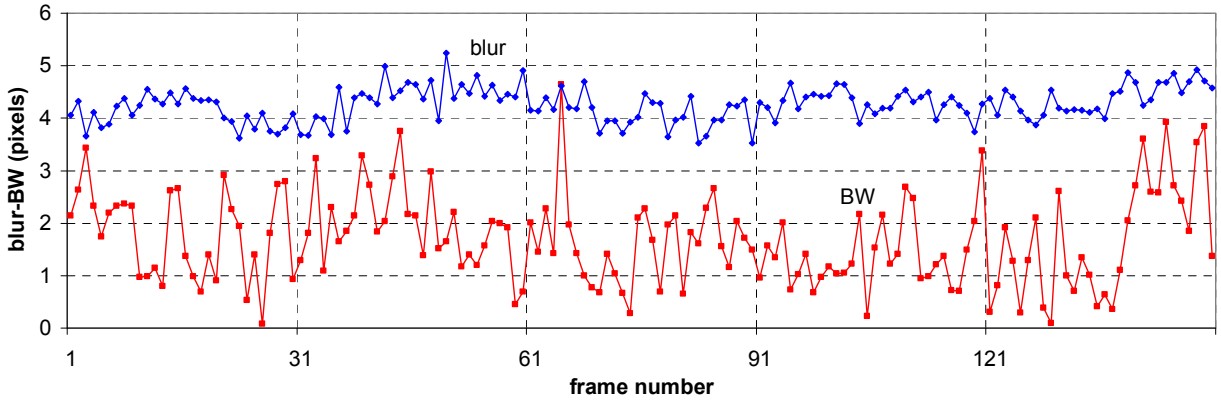

Figure 8. Example of blur and BW (in pixels) in a typical "150 frame" series on 9/4 04.00 (5 seconds of data)

wander are completely uncorrelated and that the beam wander is rapidly changing from frame to frame. The blur shows some low frequency components, which is also rather common in other series. At the time of the example the wind was blowing from the North (9.6 m/s) and the ASTD was 0.36K. The C_n^2 was 10^{-15} $m^{-2/3}$ and the atmospheric transmission was 0.15 with a scintillation index around 0.2. Additional information, that can be extracted from the same data series, is shown in Figure 9. Similar to the beam wander, the intensity is not correlated with the blur. The peak-peak variations in the intensity are much larger than the peak-peak variations in the blur. On the other hand it appears, that the correlation between the intensity and the peak signal level is quite good (correlation coefficient 0.77). The plots of the second and third moment in X and Y direction show that their mean values are roughly the same. In this example the correlation between the blur in X and Y direction (related to M_{20} respectively M_{02}) is reasonably good (correlation coefficient 0.61), but M_{30} and M_{03} appear to be uncorrelated.

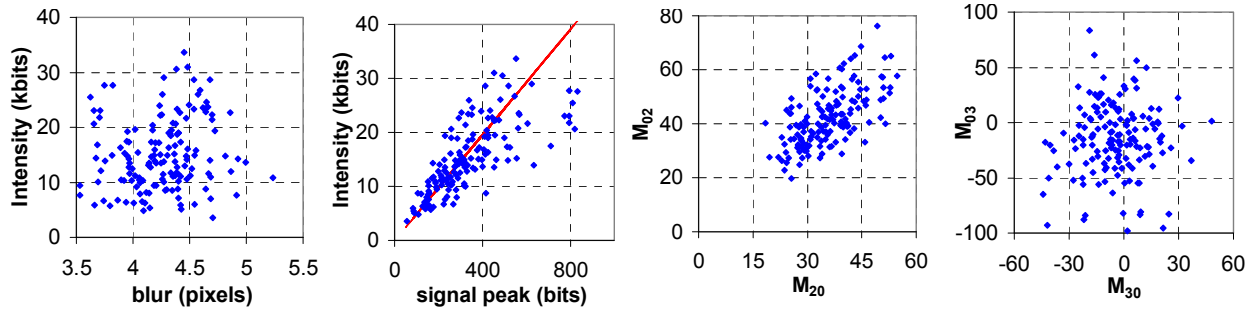

Figure 9. Characteristics of the same "150 frame" series as in Figure 8: Intensity vs blur and signal peak, M_{20} vs M_{02} and M_{30} vs M_{03}

A large number of different examples of "150 frame" series could be given, many of them with different characteristics. One of the issues is the frequent occurrence of different M_{20} and M_{02} values, contrary to the example in Figure 9. In many cases the spots seem to "breath" from frame to frame, causing distortions in the shape of the spots, changing the ratio M_{20}/M_{02} continuously. Responsible for this effect is probably refraction from large eddies, moving in horizontal and vertical directions close to the line of sight. The presence of these large eddies appears also from slow variations in blur and intensity (scale of seconds). This is in line with the fourier spectrum from the transmission data, obtained from the MSRT transmissometer [7], showing the presence of frequencies as low as 0.1 Hz.

Large scale eddies can also result in tilting of the wavefront, causing beam wander. The locality of this effect can easily be investigated by comparing the beam wander of the two central spots with a vertical spatial separation of 0.25 mrad. An example of a measurement with extremely good correlation (23/7 21.00) is shown in Figure 10. The magnitudes of BW-1 and BW-2 correlate quite good (correlation coefficient 0.94), but also the directions φ-1 and φ-2 of the tilt, which are representing the counter clockwise angles with the positive X-axis $+360^0$ (correlation coefficient 0.93).

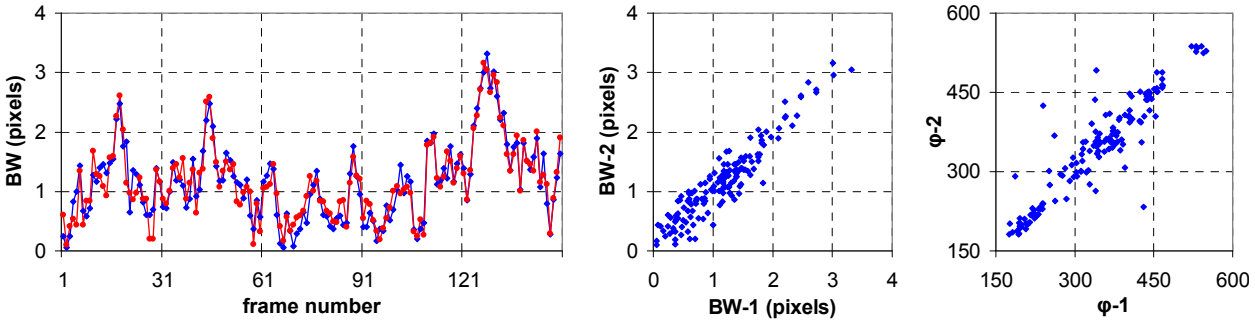

Figure 10. Beam wander in "150 frame" series of spots 1 and 2; BW-1 and BW-2 are magnitudes, φ-1 and φ-2 directions

It is noted that in this example the scintillation index, obtained from the Celestron data, was very small (<0.01) and that the C_n^2 was about 10^{-16} $m^{-2/3}$. In this situation even the blur data for both sources did correlate quite good (correlation coefficient 0.90). The intensities of both spots did not show correlation.

In normal situations the short exposure blur is only corrrelated in a small environment around the spot, the so called isoplanatic area. In the case of the range, used in FATMOSE, the diameter of this area, according to Beland [10], would be of the order of 5 to 10 µrad. It is therefore interesting to observe for conditions of low scintillation, such as in the case previously described, large areas of constant tilt (>0.25 mrad), which is attractive news for designers of adaptive optical systems, as this tilt can rather easily be corrected. It appears that a wavefront correction, applicable for one location, is also valid for other locations, separated more than 0.25 mrad.

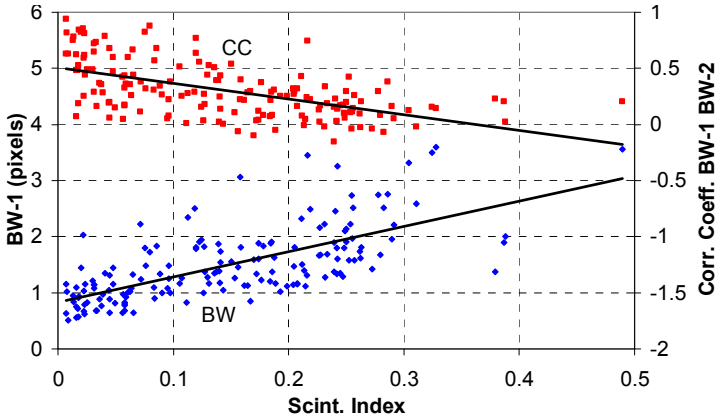

Figure 11. Beam wander for source 1 and the correlation coefficient as function of the scintillation index

In order to check the consistency of this phenomenon for other values of the scintillation index, data from the selected series, presented in Figure 6, were chosen for cases that the two central spots were selected. For these data, that contain a variety of weather conditions, the values of both beam wanders were compared. Their correlation coefficient as function of the scintillation index SI (defined here as the mean value for 150 frames of the squared ratio of the standard deviation and the mean value of the intensity I), is shown in Figure 11. It is found that the correlation is getting poor for SI values of 0.3 and higher. It is also clear that a low SI value does not guarantee a good correlation coefficient. In Figure 11 the dependence of BW as function of SI is also shown. Following are empirical relations between the correlation coefficient CC and SI and of BW and SI: CC=-1.41SI+0.51 and BW=4.50SI+0.83.

7. TIME SERIES

In this section some examples are given, showing the temporal behaviour of atmospheric turbulence effects such as blur and beam wander during a period of several days with variable weather conditions. This information is of interest for better understanding the natural variability of both effects in time, their correlation with weather conditions and their predictability. Contrary to the 475 selected events, discussed in section 5, all of them chosen in more or less stationary conditions, one is generally faced (apart from day-night changes) with frequent and rapid variations in air temperature and humidity and changes in windspeed and –directions. Two periods of five days were selected: 28 March to 1 April and 20-24 April. In both periods the two central sources were used for the determination of blur and beam wander. The blur value was calculated by averaging the blur of both sources. In some occasions around noon time, the blur value of the upper source was affected too much its the sunlit background and therefore eliminated. Some corrections had to be made for conditions with rapid changing ASTD, causing the spot running out of its window. All data, collected with a sampling rate of one set each five minutes, were averaged for a period of half an hour and sampled each 15 minutes.

Figures 12 to 14 show samples of the data set for the first period and Figures 15 to 17 show similar data for the second period. Figures 12 and 15 show the variation of blur, beam wander and scintillation index, collected with the Celestron camera and the C_n^2, collected with the BLS 900. Figures 13 and 16 show the windspeed and ASTD, collected at Roman Rock and the transmission over the 15.7 km path, collected with the MSRT transmissometer. Figures 14 and 17 show some correlation diagrams between the various collected parameters. The accuracy of the blur data is generally rather good with ratios of the standard deviation and the mean value of the blur of 10%, occasionally 20-30%. It is noted that the variations between the 5 minute samples are quite large, reason why the blur was averaged over 30 minutes.

As a consequence it is uncertain that lucky shots with 50% of the mean blur value are always present in image series of 150 frames. For beam wander the ratio of the standard deviation and the mean value is most of the time 50%. Figure 12 shows that the blur decreases roughly a factor 2 within a few days, but during the 1st of April the blur level returns to the original level. Beam wander is following the trend of the blur quite close, which is also apparent from the correlation diagram in Figure 14. It is noted that the scintillation index also follows this trend, while the C_n^2 is correlated much less. It appears that the SI from the Celestron data and from the MSRT data are well correlated for SI values lower than 0.3. The weather data and the transmission data show hardly any correlation with the blur data.

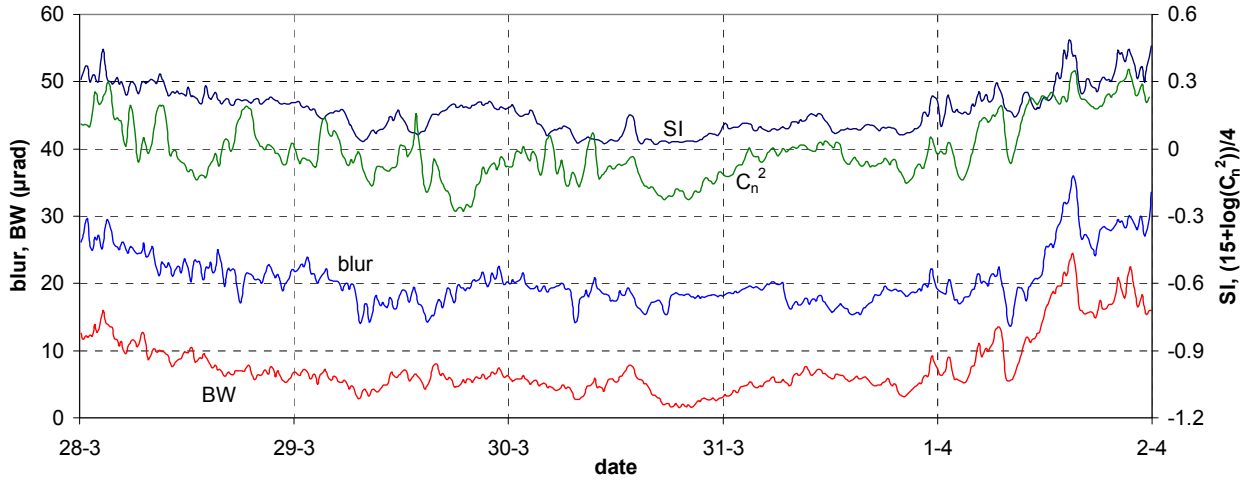

Figure 12. Blur, beam wander BW, scintillation index SI and C_n^2 data for the period 28 March to 1 April 2010

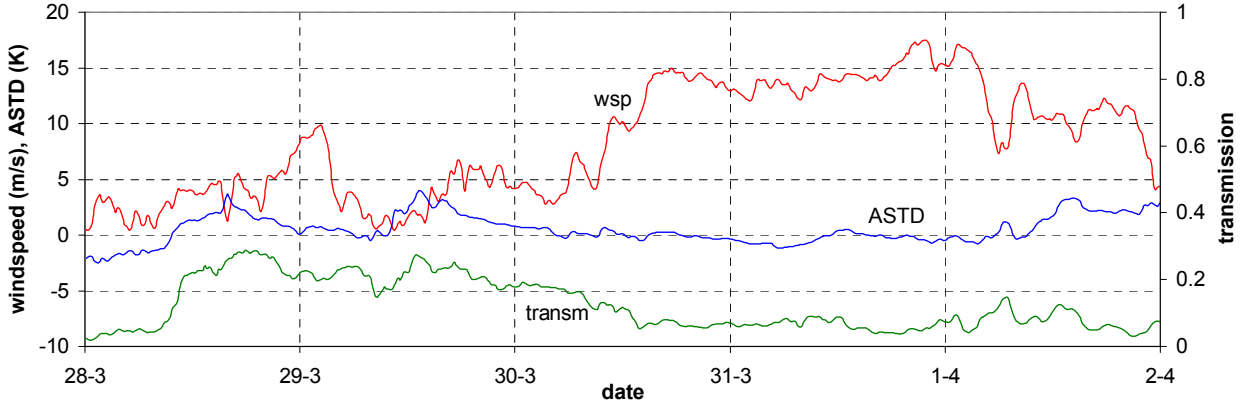

Figure 13. Windspeed and ASTD at Roman Rock and transmission (@ 0.8 μm) from MSRT along the 15.7 km path

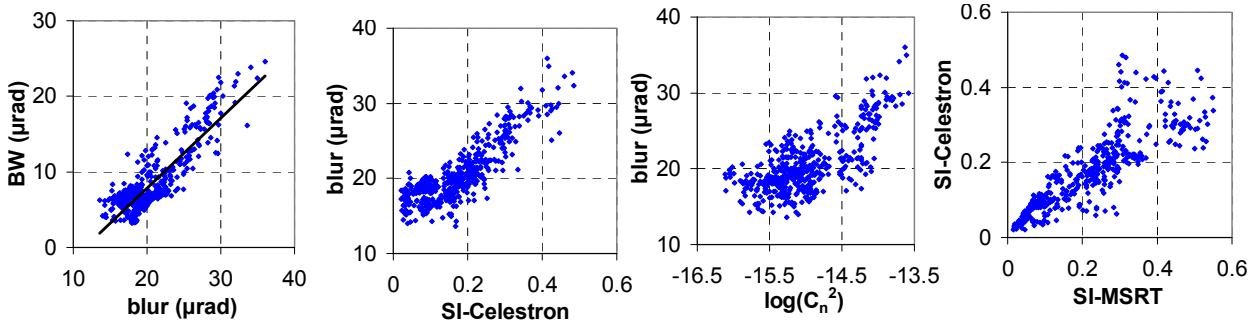

Figure 14. Correlation diagrams of blur, BW, SI and C_n^2 for the data of the first period (Figure 12)

Figure 15 shows rapid and strong variations in blur values, for example on the 21st of April, shortly after warm and dry air was moving into the area (driven by a Northerly wind), causing a drop in the blur value of about a factor 3. The same drop is found in the plots of C_n^2 and SI. The general trends of these parameters are not following closely the temporal behaviour of the blur. On the other hand blur and beam wander correlate rather good, similar to the first period. The poor correlation between the blur and C_n^2 is probably due to the variability of C_n^2 along the path. It is interesting that the correlation between BW and C_n^2 is better, probably due to the tilt mechanism of BW. It is noted, that the correlation of the SI obtained from the Celestron imagery and the MSRT (not shown here) is the same as in the 1st period.

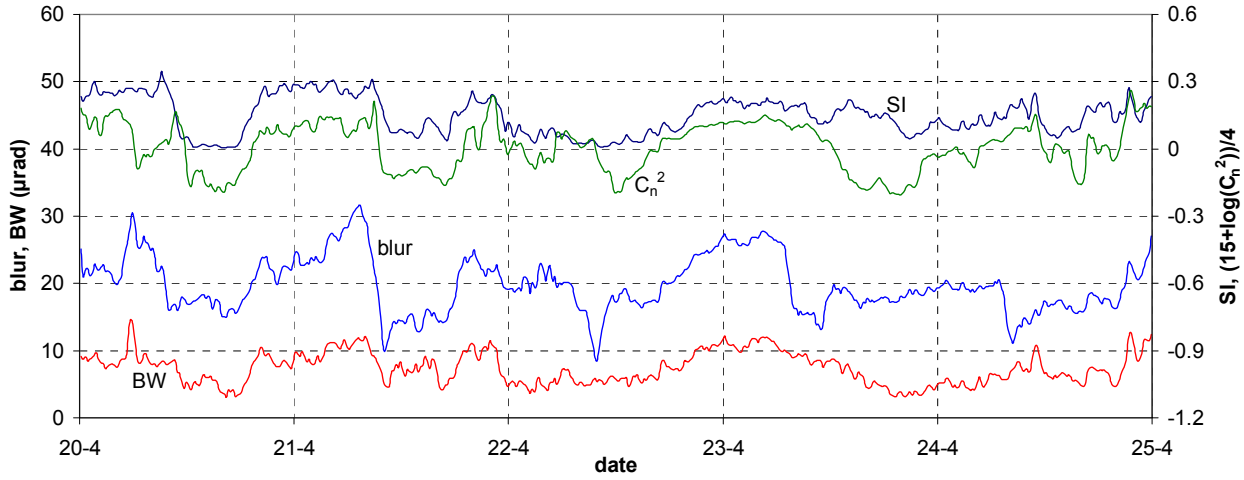

Figure 15. Blur, beam wander BW, scintillation index SI and C_n^2 data for the period 20 to 24 April 2010

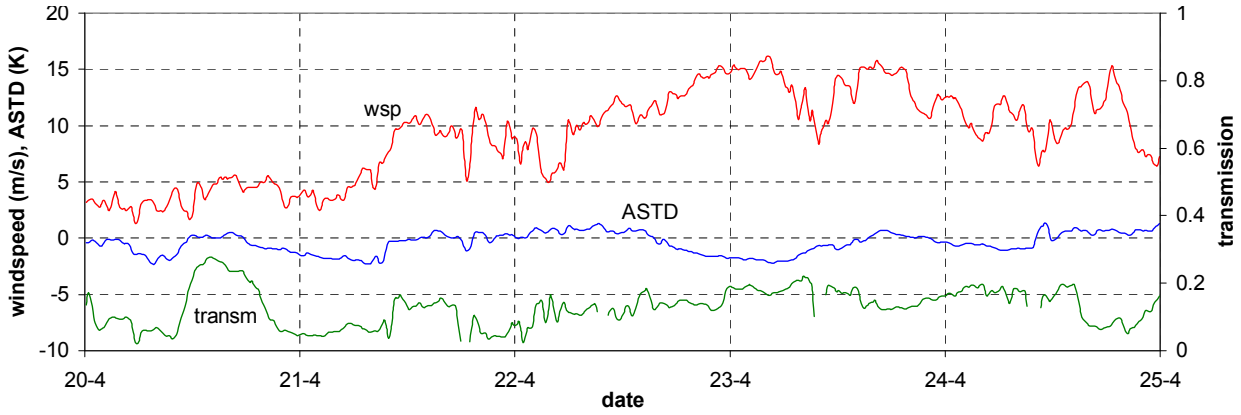

Figure 16. Windspeed and ASTD at Roman Rock and transmission (@ 0.8 µm) from MSRT along the 15.7 km path

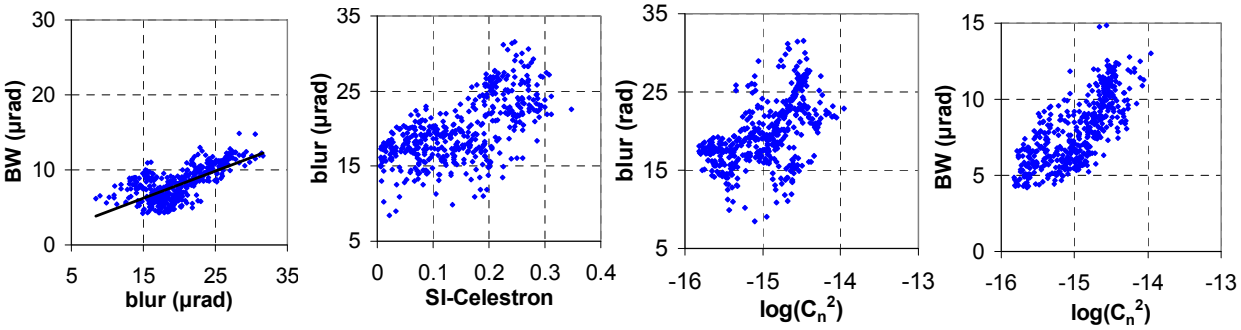

Figure 17. Correlation diagrams of blur, BW, SI and C_n^2 for the data of the second period (Figure 15)

8. COMPARISON WITH PREDICTIONS

In this section the measured data, presented in the previous sections are compared with predictions based upon the theory of turbulence, as given by Beland [10] and Ishimaru [13]. According to Fried [3], blur is determined by the atmospheric coherence length r_0, which is related to the wavelength λ, C_n^2 and the range R as given in formula (1). From this the blur σ_a can be found to be approximately:

$$\sigma_a \approx 2.1\lambda/(r_0\pi\sqrt{2}) = 2.56\lambda^{-0.2}(C_n^2 R)^{0.6}; \quad \text{for } \lambda = 0.8*10^{-6} \text{ m and } R = 15.7*10^3 \text{ m follows: } \sigma_a = 14.0*10^9 (C_n^2)^{0.6} \ \mu\text{rad} \qquad (5)$$

where the wavefronts are assumed to be plane waves. Equation (5) allows a direct comparison between the measured blur and C_n^2. From a slightly different theoretical consideration follows a relation for the beam wander BW, in which the diameter D of the receiver is taken into account:

$$BW = (2.91 D^{-1/3} C_n^2 R)^{0.5}; \quad \text{for } D = 0.2 \text{ m and } R = 15.7*10^3 \text{ m follows: } BW = 2.8*10^8 (C_n^2)^{0.5} \ \mu\text{rad} \qquad (6)$$

It is noted that the beam wander is independent of the wavelength, because it is following directly from the tilt of the wavefront. From (5) and (6) a direct relationship between blur and beam wander can be derived: $BW = 0.98(\sigma_a)^{5/6}$. For the scintillation index SI the following relation is found:

$$SI = 1.23(2\pi/\lambda)^{7/6} R^{11/6} C_n^2; \quad \text{for } \lambda = 0.8*10^{-6} \text{ m and } R = 15.7*10^3 \text{ m follows: } SI = 6.71*10^{15} C_n^2 \qquad (7)$$

It is noted here, that in the theory of turbulence effects, SI is based upon the logaritm of the intensity. The measurement results, presented so far are based upon the intensity. The difference in SI between both concepts is apparently small. From the relations (5), (6) and (7) the following direct relations between blur, BW and SI are found: $\sigma_a = 17.8*(SI)^{0.6}$ and $BW = 3.42*(SI)^{0.5}$.

A comparison of measured blur and BW data with data, predicted from equations (5) and (6) for the selected data series of section 5, is shown in Figure 18. In a first glance the correspondence between measured and predicted blur data is not large. The lowest predicted blur data are about two times smaller than the measured ones, while the largest predictions are about two times bigger. The mean values of the measured and predicted blur is however roughly the same: 20 µrad. It looks as if the small predicted blur corresponds to the measured lucky shots and the large predictions to the poorest ones.

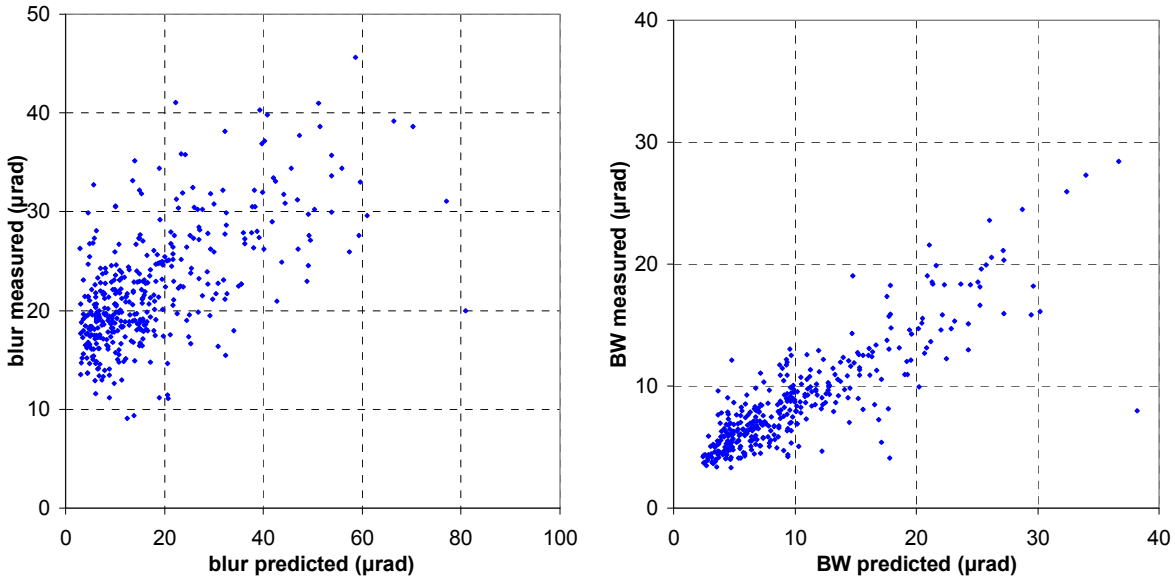

Figure 18. Comparison of predicted and measured blur for selected data series over the total FATMOSE period

The plot at right of Figure 18 shows a linear relationship between the measured beam wander (BW_m) and the predicted beam wander (BW_p): $BW_m=0.57*BW_p+2.97$ with a correlation coeficient of 0.88. It appears again, as in Figure 11, that beam wander is behaving more linear with respect to environmental parameters such as SI and C_n^2. It is clear, that the predicted BW is roughly a factor 1.6 bigger than the measured BW. A similar result is obtained from the time series, presented in section 7, for which the correlation plots are shown in Figure 19. For the combined 10 days of data, the following linear relationship is obtained: $BW_m=0.44*BW_p+3.53$ with a correlation coefficient of 0.87. Less correlation is again found for the measured and predicted blur with less blur for smaller values and more blur for larger values. It is interesting to note that the mean values of the predicted and measured blur for this combined time series (960 data points) do not differ that much: 18.0 respectively 20.1 μrad, which corresponds to a C_n^2 value of 10^{-15} $m^{-2/3}$. For the selected data series presented in Figure 18 (475 data points) the mean blur values are: 19.3 respectively 22.6 μrad. It is reminded (see sections 4 and 5) that these measured and predicted mean blur values of roughly 20 μrad correspond with an atmospheric resolution of about 50 μrad. From the prediction of the atmospheric coherence length r_0 in equations (1) and (5) follows that for σ_a values between 10 and 40 μrad, r_0 varies between 3.8 respectively 0.95 cm.

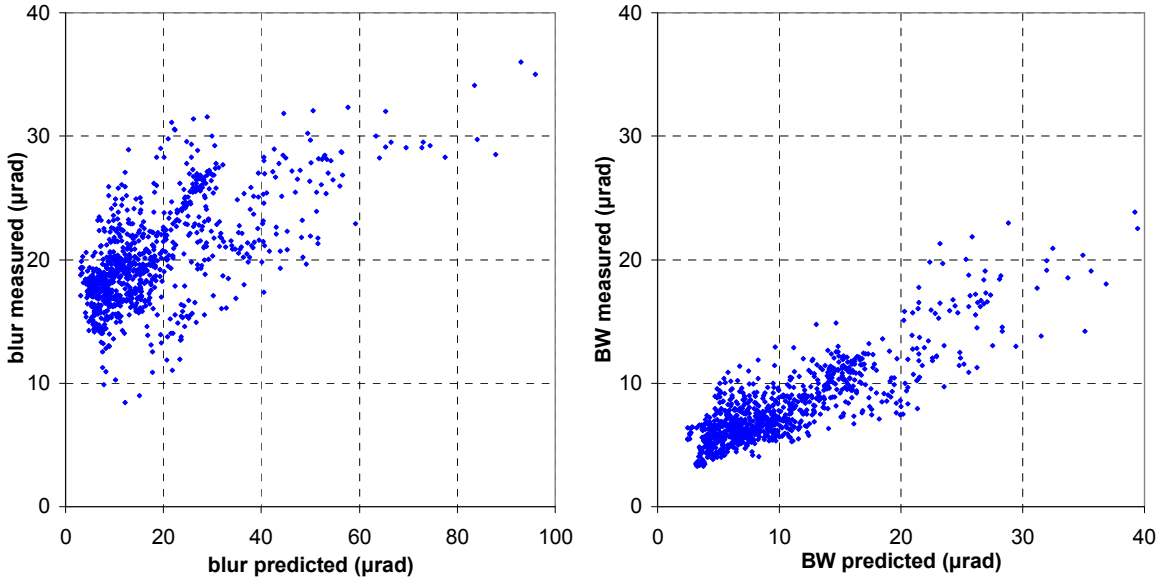

Figure 19. Comparison of predicted and measured blur and BW data for the time series of 28/3 to 1/4 and 20/4 to 24/4

It is found, that the spread in the blur data, compared to the C_n^2 based predictions is considerable. This is similar to the experience with the refraction data [8], where it was found that the ASTD in the False Bay is not constant along the path. In the derivation of formulas (5)-(7), C_n^2 is assumed to be constant along the path. According to the marine boundary layer theory C_n^2 is dependent on the vertical exchange of heat and momentum fluxes, which are dominated by the ASTD. Predictions based upon one value for C_n^2 are basically not correct. It is interesting however to note, that the mean blur value for series of measurements over longer periods does correspond quite good with its mean predicted value. The spread in the beam wander data is less than the spread in the blur data, which is probably due to the main mechanism for beam wander, being the larger eddies. It is possible that these eddies are mainly present in the area close to the receiver (with coastal mountains) where the scintillometer was located.

The interpretation of formula (7) for the scintillation index introduces some problems, because during its derivation it was assumed that the receiver and the source both have very small apertures, in any case smaller than the atmospheric correlation width. It is well known [14] that in case of larger apertures, as used in the FATMOSE set-up, considerable aperture averaging can occur, decreasing the irradiance fluctuations. As a result the SI is degraded by a certain factor, determined by the transverse coherence length ρ_0 ($=r_0/2.1$) and the receiver aperture. It is noted, that the derivation of equation (7) is made under weak turbulence conditions. In the FATMOSE set-up this probably occurs very seldom due to the long range (15.7 km) and mean C_n^2 values of around 10^{-15} $m^{-2/3}$. For achieving weak turbulence conditions the C_n^2 value should be in the FATMOSE set-up 10^{-16} or less. In other turbulence conditions there may be so called saturation,

where the value of SI remains constant above a certain level[15]. If in equation (7) C_n^2 equals 10^{-15} $m^{-2/3}$, the resulting SI value becomes 6.71, which is about 30x larger than the measured SI value in the same conditions. One might conclude that the measured SI value are useless in the interpretation process for blur and BW. Nevertheless it appears from Figures 14 and 17, that the blur is corresponding more or less linearly with the measured SI values (not shown in this paper). The same holds for the relation between BW and the measured SI as well as for the relation between SI and C_n^2, both for the selected data series as for both time series. The measured SI data are therefore still making sense, as saturation was not observed. In practical situations one might use cameras such as the Celestron with Marlin sensor to observe and measure the scintillation from distant lamps over water, determine the SI and estimate the corresponding blur and BW, using equations (5) to (7).

9. DISCUSSION AND CONCLUSIONS

In this paper a simple experiment is described, providing direct information on the resolution of a camera system by using a bar pattern and investigating the frequency which is just discernable. The resolution, limited by atmospheric turbulence, is succesfully verified with predictions from theory. This method for determination of atmospheric resolution is not suitable for long term measurements. For this purpose, a set-up was realised in the False Bay (South Africa), where a set of point sources was used to measure the atmospheric LSF. It appeared that most of the time this LSF has a nearly Gaussian shape, so has its Fourier transform. A method has been described to obtain the atmospheric blur directly from the LSF after correction for the camera blur. It was also described, how simultaneously the beam wander characteristics were determined for series of images, taken each five minutes during more than 300 days. The statistics of the properties of blur and beam wander are of great interest for the user of electro-optical sensors in coastal areas. It was found from a representative set of data, that the mean values for blur and beam wander are 22 respectively 9 μrad, with maxima and minima of about a factor 2 around these values. It was indicated how to interpret these values by taking the separation distance (in μrad) of two point sources that are just discernable, which distance appears to be a factor 2.43 bigger than the blur value. The associated atmospheric MTF is related to σ_a by the equation: $F(f)=\exp\{-2(\pi\sigma_a f)^2\}$, which reaches its 1/e value at the spatial frequency: $f=1/\pi\sigma_a\sqrt{2}$.

The beam wander (BW) characteristics, being important for the application of adaptive optical systems, were analysed for two sources, vertically separated 0.25 mrad. It appeared that in conditions of small turbulence (low value of SI), the BW of both sources is strongly correlated, indicating that wavefront corrections for one source are also applicable for its surroundings. For the representative selected data set the relation between the correlation coeficient and the BW and the SI value was determined. From the analysis of the “150 frame series” it appeared that the correlation between blur and spot intensity is generally poor, but the blurs in X and Y direction are generally moderately correlated. It was found that blur and BW are completely uncorrelated in the “150 frame series” and that in many cases the blur as well as the BW contain low frequency components, indicating the presence of large eddies. Another issue is the variation of blur and BW in the series of 150 frames, which appears to be about 20% for the blur and 50% for the BW. Actually some of the 150 frames may show up with blur values, less than 50% of the mean. For these frames, where one could speak about “lucky shots”, the image is locally sharper, but only in a small area around the point source, the so-called isoplanatic area.

Blur and BW data, accompanied by weather data, have been presented for two time series, each covering five days of measurements. From these plots it appears to be difficult to understand the variation of blur with time. One of the reasons is that the weather data (including C_n^2 data), collected close to the Line of Sight, are probably not constant along the full range of 15.7 km. Similar to the selected data series a good correlation was found between blur and BW, following the relation: blur=0.96BW+12.8 with a correlation coefficient of 75%. A good correlation was also found for the scintillation index SI, as measured by the imaging Celestron camera and the MSRT transmissometer: SI-Cel.=0.64(SI-MSRT)-0.033 with a correlation coefficient of 0.86. This is a bit remarkable, as the aperture of the Celestron is 200 mm and for the transmissometer 38 mm, resulting in different aperture averaging. In addition it appeared that blur and SI are reasonably to well correlated by the relation: blur=32SI+15 with a correlation coefficient of 73%. The correlation between blur and C_n^2 for the selected data series was moderate: $\text{blur}=7.7\log(C_n^2)+139$ with a correlation coefficient of 61%. For the first time series with smoothly variable weather conditions the correlation between blur and C_n^2 was somewhat different: $\text{blur}=5.1\log(C_n^2)+97$ with a correlation coefficient of 72%. For the second time series the correlation between blur and C_n^2 was found to be less: $\text{blur}=5.3\log(C_n^2)+99$ with a correlation coefficient of 0.54. This smaller correlation is due to the rapidly changing weather conditions in this period.

The comparison of blur measurements and predictions showed a good agreement of the mean values over longer periods, as well for the selected data series as for the two five-day series. Although the weather conditions are variable along the path, the means are adequately averaged out. It was found however that the predictions are not correct concerning the minimum and maximum blur values. While the measured blur values stay within 10 and 40 μrad for the selected period, the predicted blur (based upon C_n^2 input) varies from 5-80 μrad. It appears that this predicted minimum and maximum corresponds roughly to the blur extremes in the 150 frame series. The measured beam wander appears to be significantly smaller than the predicted beam wander (based upon C_n^2 input) for all periods. No explanation has been found for this behaviour so far. Predictions concerning scintillation are resulting in much higher predicted (factor 30) than measured SI data. This is a result of the averaging effect of the receiver aperture. From the blur measurements it was found that r_0 is predicted to be ranging from 3.8 to 0.95 cm, so the transverse coherence lenth ρ_0 varies from 1.8 to 0.45 cm. Considering the aperture diameter of the Celestron (20 cm), it seems realistic to expect a factor 11 to 44 SI reduction, taking the ratio of the aperture and ρ_0.

We want to thank Michael Saunders (Station 16 Commander) and Mario Fredericks (Station 16 Deputy Commander) from the National Sea Rescue Institute for permission for mounting the sources on the building at Strandfontein and their support during the trial. We further thank Peter Fritz, Leo Cohen, Marco Roos and Koos van der Ende of TNO for their support in preparing the hardware and software for the FATMOSE trial.

10. REFERENCES

[1] Arie N. de Jong et al, *Measurement of optical refraction-, transmission- and turbulence effects in the False Bay, South Africa; June 2007*; SPIE Volume 7108, Optics in Atmospheric Propagation and Adaptive Systems XI, Cardiff, September 2008

[2] Arie N. de Jong et al, *Optical characteristics of small surface targets, measured in the False Bay, South Africa; June 2007;* SPIE Vol. 7300, Infrared Imaging Systems; Design, Analysis, Modeling and Testing XX, Orlando, April 2009

[3] David L. Fried, *Optical resolution through a randomly inhomogeneous medium*, JOSA, **56**, 1372-1379 (1966)

[4] Gerald C. Holst, *Electro-Optical Imaging System Performance (3rd ed.)*, SPIE Press Monograph PM 121, 2003

[5] A.M.J. van Eijk et al, *EOSTAR Pro: a flexible extensive library to assess EO sensor performance*, SPIE Volume 7828, Optics in Atmospheric Propagation and Adaptive Systems XIII, Toulouse, September 2010

[6] Arie N. de Jong et al, *Preliminary results of the FATMOSE atmospheric propagation trials in the False Bay, South Africa, November 2009-July 2010*, SPIE Volume 7828, Optics in Atmospheric Propagation and Adaptive Systems XIII, Toulouse, September 2010

[7] Arie N. de Jong et al, *Application of year-round atmospheric transmission data, collected with the MSRT multiband transmissometer during the FATMOSE trial in the False Bay area*, SPIE Volume 8161, Atmospheric Optics: Turbulence and Propagation, San Diego, August 2011

[8] Arie N. de Jong et al, *Marine boundary layer investigations in the False Bay, supported by optical refraction and scintillation measurements*, SPIE Volume 8178, Optics in Atmospheric Propagation and Adaptive Systems XIV, Prague, September 2011

[9] Arie N. de Jong et al, *TG16 point target detection experiment POLLEX, Livorno 2001,* SPIE Volume 4820, Infrared Technology and Applications XXVIII, Seattle, July 2002

[10] Robert R. Beland, *Propagation through Atmospheric Optical Turbulence*, The Infrared & Electro-Optical Systems Handbook, Volume 2, SPIE Optical Engineering Press, 1993

[11] Karin R. Weiss-Wrana, *Turbulence statistics in littoral area*, SPIE Volume 6364, Optics in Atmospheric Propagation and Adaptive Systems IX, Stockholm, September 2006

[12] Arie N. de Jong et al, *Alternative measurement techniques for infrared sensor performance*, Opt. Eng. **42**(3) 712-724 (March 2003)

[13] Akira Ishimaru, *Wave Propagation and Scattering in Random Media, Volume 2, Multiple Scattering, Turbulence, Rough Surfaces and Remote Sensing*, Academic Press 1978

[14] Larry C. Andrews and Ronald L. Philips, *Laser Beam Propagation through Random Media, 2nd ed.* , SPIE Press, Bellingham USA, 2005

[15] Robert S. Lawrence and John W. Strohbehn, *A Survey of Clear-Air Propagation Effects Relevant to Optical Communications,* Proc IEEE, Vol. 58 No. 10, October 1970